Touching the sound: Audible features enable haptics for robot control

Hongshen Shi, Matteo Russo, Juan de la Torre, Abdelkhalick Mohammad, Xin Dong, Dragos Axinte

***Abstract*—Haptic control interfaces can significantly improve the quality of teleoperation in robotic and mechatronic systems. However, the required force feedback introduces new challenges when highly constrained environments and systems hinder the use of conventional force sensors. In this paper, we propose a haptic control method that provides feedback to the operator when force data can be extracted from a sound signal. As sound can be acquired by a microphone deployed outside the workspace, this method enables remote feedback in any process that can be characterized through acoustic emissions (e.g. machining), without the need for sensors embedded in the system or deployed in the work environment. The performance of the method is verified by an example application, with a teleoperated robot that executes a machining process (milling and grinding), whose sound is acquired with a microphone and processed to successfully estimate the machining force for haptic feedback.**

***Index Terms*—Haptics, force feedback, bilateral control, audible sound features, force measurement.**

I. Introduction

HAPTICS improve teleoperation quality by enhancing user experience with tactile and force feedback [1]-[4]. Haptic devices have been extensively used in many fields, from medicine [5] to industry and service. Measuring the forces acting on the teleoperated system is at the core of haptics. When feasible, an onboard force sensor enables a direct force estimation. However, many applications prevent this approach because of, for example, space constraints (e.g. microrobots), hazardous environments (e.g. radioactive), and unreliability of conventional sensors (e.g. continuum/compliant robots, where a force sensor on the tip would measure not only external forces but also internal reaction forces due to the elasticity of the system, corrupting or hiding the actual external load).

To address those cases, indirect force sensing is widely researched to extract the load acting on the system through a different kind of measurement. For example, Fiber Bragg Grating (FBG) can sense force through optical features [6]-[8]. However, FBG sensors must be embedded in the robot's body [9] or end-effector [10][11]. This requires the robot to be designed or modified to integrate the sensors, which could be unfeasible or highly expensive. As an alternative, vision-based force measuring methods use the deformation of the robot's structure [12] or surroundings [13] caused by contact forces to estimate the force exchange. However, this method requires at least one of the contact surfaces to be soft enough to obtain visible deformation and assumes unhindered line of sight. Other applications employ "remote" force measurements to estimate the load acting on the end-effector of a robot. This is done for example in tendon-driven continuum robots, where load cells at the tendons are used to estimate the force at the tip [12]-[14]. This method is only accurate in specific conditions (i.e. external load comparable with tendon tension), as the load could be "hidden" by signal noise and other factors. Furthermore, an accurate dynamic model of the robot is required, and solving this model could prevent real-time applications.

More extreme cases, such as operation in radioactive environments [15][16] or in extremely confined spaces (e.g. aeroengines [17]), could prevent the use of onboard sensors altogether. When these operations generate an audible sound, however, this acoustic signal can be acquired with an external remote system and processed to extract information from the operation itself. For example, in machining [18] the frequency signatures of audible sounds have been shown to identify cutting [19], sawing [20], milling [21], and grinding [18] parameters, or evaluate surface quality [22].

These examples show that acoustic met

hods can be successful in acquiring process information from audible features. We thus propose in this work a haptic system that provides feedback in scenarios where the work environment cannot be accessed nor seen, but where a sound proportional to process force/torque can be acquired remotely. This method is independent from the system, as it does not require any hardware modification. As illustrated in Fig. 1, a haptic interface works as leader device to send motion command and control a follower robot. Meanwhile, process sound is acquired and used to extract the interaction force from its audible features. The system identifies the corresponding force feedback and realizes it with the haptic interface. An overview of the control method is reported in Section II. In Section III, an example of the proposed system is reported for an aerospace repair application, with the robot in Fig. 1 guided in a machining operation through a haptic device. In Section IV, an experimental validation is presented for different machine tools and workpiece materials, and the results are discussed.

The main contribution of this paper is represented by the development of a method that generates haptic feedback for any sound-generating process in which the force is proportional to the acoustic emission (e.g. machining). The main challenge behind the proposed method is processing the sound signal for

Submitted for review on XX/XX/2022.

This work was supported by Rolls-Royce plc.

H. Shi, M. Russo, J. de la Torre, A. Mohammad, X. Dong, and D. Axinte are with the Rolls-Royce UTC in Manufacturing and On-Wing Technology, Faculty of Engineering, University of Nottingham, Nottingham NG8 1BB, United Kingdom (e-mail: {hongshen.shi; matteo.russo; abd.mohammad1; xin.dong; dragos.axinte}@nottingham.ac.uk).

real-time feedback: previous works demonstrated the feasibility of using sound to estimate force features [18], but could not provide the high frequency needed for haptic feedback and depended on "ideal" acquisition conditions (microphones nearby the process, controlled background noise, no noise or disturbance from a tailored experimental setup). In this paper, we solve these challenges to enable haptic teleoperation with the proposed method, significantly increasing the refresh rate of the sound processing algorithm and improving stability in presence of noise. This method can be adapted to monitor any process in which a desired characteristic can be extracted from sound. As a single microphone, which can be placed remotely, is needed to acquire sound, the method has a significant advantage in removing the need to assemble onboard sensors, which could not fit or involve significant costs.

II. System Overview

The system proposed herein aims at enabling teleoperation with haptic feedback for a robot that cannot use conventional force sensors either for system requirements or environmental constraints. To this end, we propose using audible process features to generate haptic feedback. The user could then sense the robot through a single remote microphone.

The system is composed by three main parts, as shown in Fig. 2: robot control, haptic interface, and sound signal processing. The robot control block (A) receives commands from the haptic device and controls the robot's actuators accordingly. The sound signal processing block (B) acquires the sound generated by the target operation and extracts force in real time. The haptic interface block (C) acquires the user's motion input while providing them with force feedback in real time.

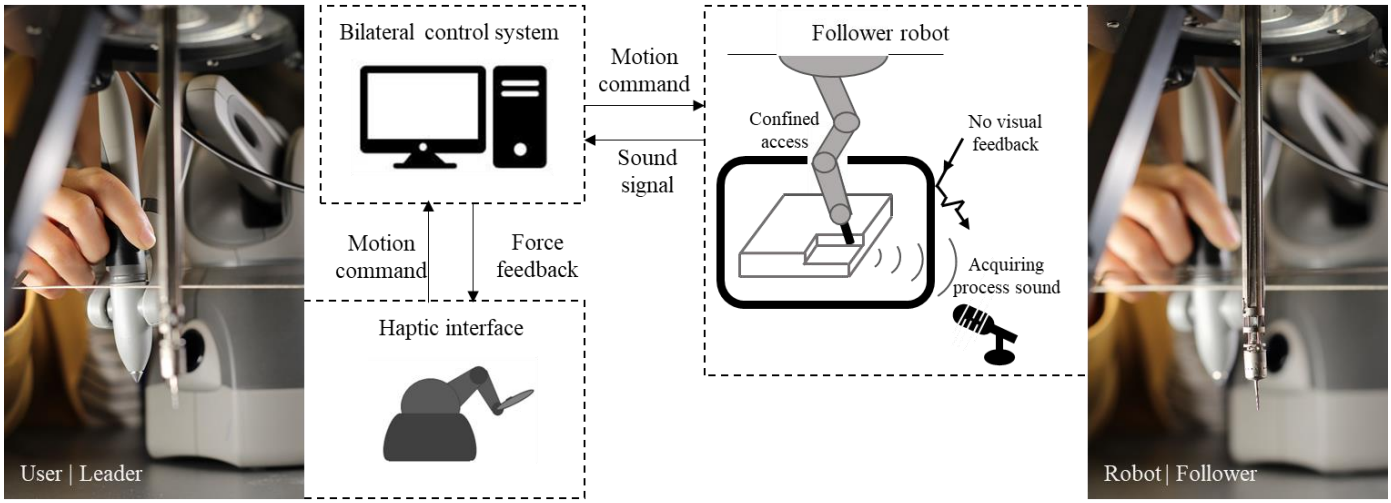

Fig. 1. Obtaining haptic feedback from audible sound features: a conceptual diagram.

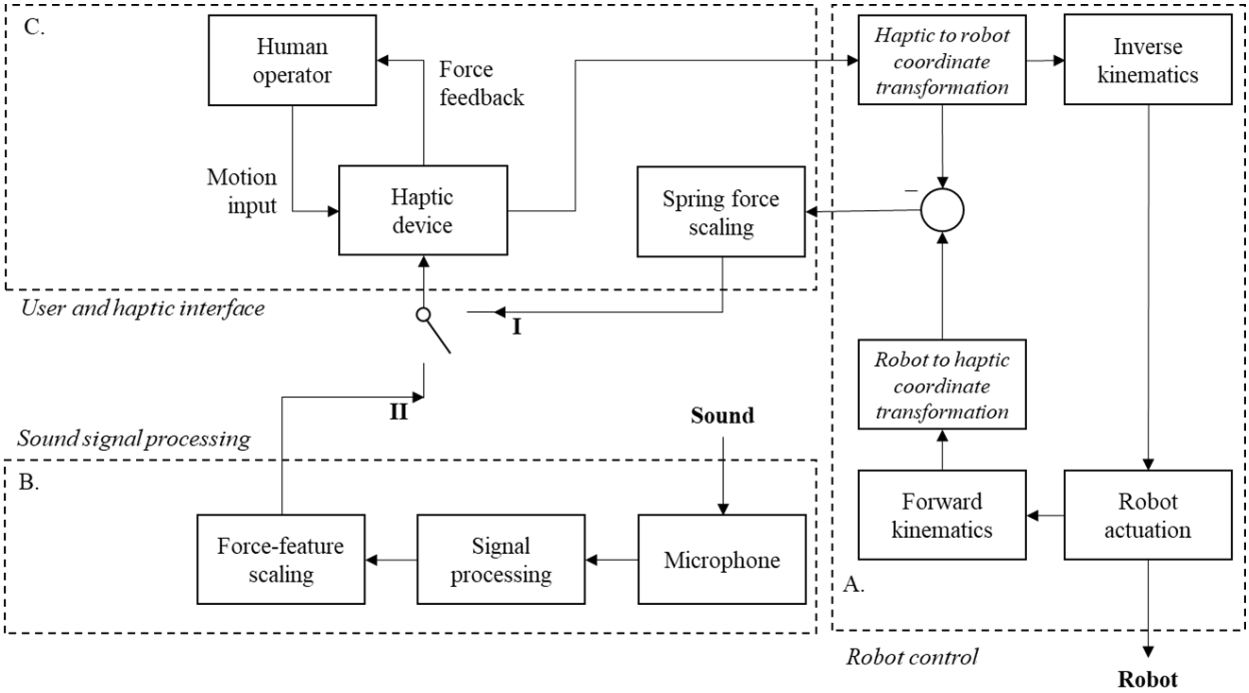

Fig. 2. Control architecture of the proposed system: robot motion control in block A; sound signal acquisition and processing in block B; haptic interface in block C, with a switch between motion control without sound feedback (line I) and motion control with sound feedback (line II).

The system can switch between two feedback modes: *motion control* mode (switch in block C linked to I), when no process sound is detected, or *touching the sound* mode (switch linked to II), when an acoustic emission within the process's range is acquired. In case I, the haptic interface provides force feedback only to limit a sudden input motion that cannot be followed by the robot because of speed limits, collisions, or safety. As such, the haptic interface in this mode provides a force proportional to the difference between the current position of the robot and the desired one commanded by the haptic: the larger the difference between the robot's current and desired positions, the larger the force needed to move the robot further. In case II, the system is *touching the sound*. In this mode, the acoustic emission is processed to derive the interaction force between the robot's end-effector and the environment, which is then scaled and returned to the user as feedback on the process.

A. Robot motion control

When the system is in *motion control* mode, the user inputs the motion command from the haptic interface by changing the position and orientation $\{P_I, R_I\}$ of the haptic device's control bar, described by position vector $P_I \in \mathbb{R}^3$ and rotation matrix $R_I \in SO(3)$. A transformation matrix $T_{IE} \in SE(3)$ is used to map the haptic device workspace in the robot end-effector workspace as position vector $P_E \in \mathbb{R}^3$ and rotation matrix $R_E \in SO(3)$. Thus, the commanded end-effector position in the robot coordinate system $\{P_E, R_E\}$ can be calculated from the pose of the haptic device as

$$\begin{bmatrix} R_E & P_E \\ 0 & 1 \end{bmatrix} = T_{IE} \begin{bmatrix} R_I & P_I \\ 0 & 1 \end{bmatrix}. \tag{1}$$

Then, to drive the actuators of the robot, the joint positions $\{l_1, l_2, \cdots, l_n\}$, where n is the number of degrees of freedom of the robot, are calculated according to the robot inverse kinematics. This command process is shown in Fig. 3a.

A mismatch between the desired position (defined by the haptic input) and the output motion of the follower robot signals that the user is sending an unexpected command out of the robot's motion range in either position or velocity. As such, this error between the commanded and current position of the robot is monitored in real time, and a proportional force feedback is generated to dampen or inhibit any motion which would increase the error. In every control loop of the robot *motion control* mode (in block C, Fig. 2), the haptic device send its current position $\{P_I^M, R_I^M\}$ as motion command to the robot, and then reads the current position of robot actuators $\{l_1^S, l_2^S, \cdots, l_n^S\}$ to obtain the current position of robot end-effector.

In block B (Fig. 2), a user can choose how much they want to "feel" this pose discrepancy with the haptic device through the virtual coupling method that is used to generate the force feedback. As shown in Fig. 3b, based on the inverse process of Fig. 3a and the current position of the robot's actuators $\{l_1^S, l_2^S, \cdots, l_n^S\}$, the current pose of the robot's end-effector is mapped into the haptic device coordinate system as $\{P_I^S, R_I^S\}$. Using a user-adjustable stiffness matrix $A_I = \{A_I^F, A_I^M\}$ to scale the spring-like force generated by the position error between $\{P_I^M, R_I^M\}$ and $\{P_I^S, R_I^S\}$, a feedback wrench $W_I = \{F_I, M_I\}$ is generated as

$$\begin{aligned} F_I &= A_I^F (P_I^S - P_I^M) \\ M_I &= A_I^M R_I^S R_I^{M-1} \end{aligned} \tag{2}$$

where F_I is the feedback force and M_I is the feedback moment.

TABLE I
NOMENCLATURE

Variable	Description
	System Overview
P_I	Input position of the haptic device (haptic frame)
R_I	Input orientation of haptic device (haptic frame)
P_E	Desired end-effector position (robot frame)
R_E	Desired end-effector orientation (robot frame)
T_{IE}	Transformation from haptic to robot frame
l_i	Desired position of robot actuators
n	Number of degrees of freedom of the robot
P_I^M	Current position of the haptic device (haptic frame)
R_I^M	Current orientation of haptic device (haptic frame)
l_1^S	Current position of robot actuators
P_I^S	Current robot end-effector position (haptic frame)
R_I^S	Current robot end-effector orientation (haptic frame)
A_I^F	Force stiffness matrix for motion control
A_I^M	Moment stiffness matrix for motion control
W_I	Haptic feedback wrench from motion control
F_I	Haptic feedback force from motion control
M_I	Haptic feedback moment from motion control
W_E	Wrench applied to the robot end-effector
F_E	Force applied to the robot end-effector
M_E	Moment applied to the robot end-effector
C_i	Measurable sound feature
$W_{E,i}$	Components of W_E related to C_i
g_S	Mapping function between sound feature and robot wrench
τ	Spindle torque
ω	Spindle rotation velocity
f	Sound wave frequency
W_s	Haptic feedback wrench from *touching the sound*
A_S	Scaling factor for *touching the sound* wrench
	Robot teleoperation
θ_i	Bending angle of the i^{th} compliant joint of the robot
L	Actuation of the linear drive of the robot
t_x	Scaling factor from θ_1 to the X-axis of the haptic device
t_y	Scaling factor from θ_2 to the Y-axis of the haptic device
t_z	Scaling factor from L to the Z-axis of the haptic device
	Haptic feedback
F_H^I	Haptic feedback force for the example system
P_H^E	Haptic device position vector (haptic frame) calculated from the current robot actuation
P_H^I	Commanded position (haptic frame)
k_I	Scaling factor for motion control mode
F_M	Radial machining force
R_{EtoH}	Rotation matrix from robot to haptic frame
k_{II}	Scaling factor of machining force feedback
P_H^S	Haptic device position when entering an alert area
k_{III}	Stiffness of the haptic "virtual wall"
r	Haptic device motion direction
R	Force vector mapped in the haptic frame
	Sound tracking algorithm
f_{en}	Environment noise frequency upper limit (1000Hz)
$f_{p,i}$	Frequency with highest amplitude in the current loop
$f_{p,i-1}$	Frequency with highest amplitude in the previous loop
Δ	Frequency change limit in consecutive loops (250Hz)
$f_{out,i}$	Output spindle frequency in the current loop
$f_{out,i-1}$	Output spindle frequency in the previous loop

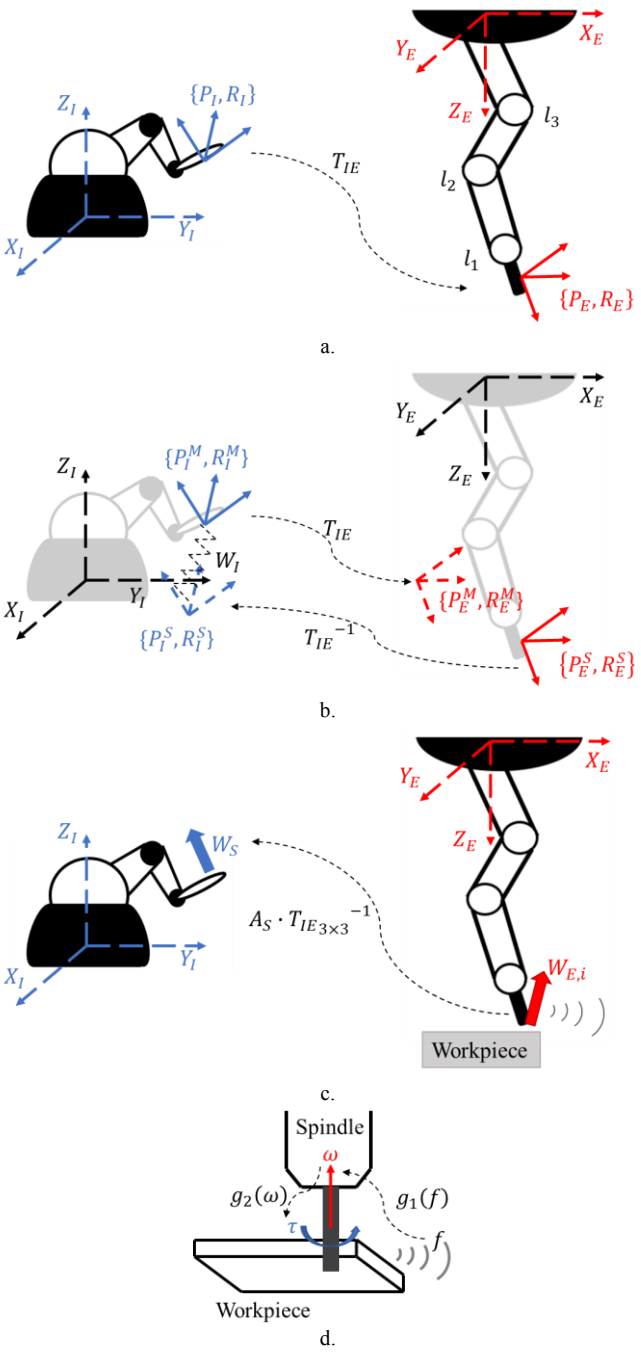

Fig. 3. Mapping between haptic device and follower robot: a. Ideal behavior of the system, with the robot always following the haptic device's motion according to the desired kinematic mapping; b. Robot *motion control* mode, with a spring-like force generated to make the user aware of a difference between the pose commanded through the haptic device and the actual pose of the robot; c. *Touching the sound*, with the user experiencing a force feedback based on process sound features; d. An example of haptic feedback acquisition from sound, with an air-driven machining process in which the spindle torque τ can be directly derived from sound frequency f as $\tau = g_2(\omega) = g_2(g_1(f))$.

B. *Touching the sound*

When the robot is executing a sound-generating tasks, such as machining, grinding, or polishing, some audible features (e.g., frequency, amplitude) are due to the interaction force between the robot's end-effector and the workpiece, as reported in the examples in [18][22][23]. The wrench applied to robot's end-effector is defined as $W_E = \{F_E, M_E\}$, where F_E and M_E are respectively the force and the moment applied to the end-effector. When a relationship between any of the components of W_E and one or more sound features $C_{sound} = \{C_1, C_2, \cdots\}$ is established, a mapping function g_S can be derived to estimate one or more components of W_E (defined by index i) as

$$W_{E,i} = g_S(C_{sound}). \quad (3)$$

A practical example of (3) is given by the a near linear relationship between spindle torque τ and spindle rotation velocity ω in air-driven spindles for machining tools [23]. The machining sound generated from interaction between tool and workpiece has a soundwave frequency f directly proportional to ω. Thus, the relationship between spindle torque τ and sound frequency f can be obtained as in Fig. 3d.

Based on the above theory, the *touching the sound* mode builds the bridge between haptic feedback and process sound. When the system turns into this mode, the process sound is acquired by a remote microphone and processed to extract relevant features. Then, according to the mapping function between force and sound features, previously calibrated, the interaction force is calculated in real time (block B of Fig. 2). After the wrench acting on the robot is evaluated, the haptic wrench W_s is obtained by scaling the measuring force as

$$W_S = A_S \cdot T_{IE}^{-1} \cdot W_E \quad (4)$$

where A_S is a user-defined scaling factor of the measured force (similarly to A_I), as shown in Fig. 3c.

III. An Example: Haptic Control of Machining Tasks

To validate the proposed method, we report an example in which the robot executes a machining operation for the teleoperated repair of aeroengine components. In this scenario, no onboard or environmental sensors can be used, as the space allowed by narrow access ports (<15 mm in diameter) is taken by robot and tool actuation. The following section details a solution to realize haptic control with the proposed method.

A. *System hardware*

The system hardware, shown in Fig. 4, is composed by three main parts corresponding to the control blocks of Fig. 2. A first subsystem with a microphone array and signal processing hardware acquires and processes sound. The haptic device acts as interface for human-robot interaction, receiving motion commands and providing force feedback. The last subsystem is a teleoperated robot with a machining tool as end-effector.

1) *Sound acquisition and processing*

This first subsystem records sound and extracts relevant features to estimate the machining force. In the reported setup, a 40PH CPP free-field array microphone with 12AL CPP pre-amplifiers (G.R.A.S. Sound&Vibration, frequency range 0-20 kHz) measures the sound spectrum. The microphone is connected to an EMP373 portable computer (ACME) equipped with a PCI-6229 IO board (16 bit, 250 kS/s) and a BNC-2110 BNC breakout board (National Instruments). Data points are acquired at 50 kHz. The machining sound spectrum is then post-processed to identify the spindle rotation frequency in real-time and estimate the interaction force through (3).

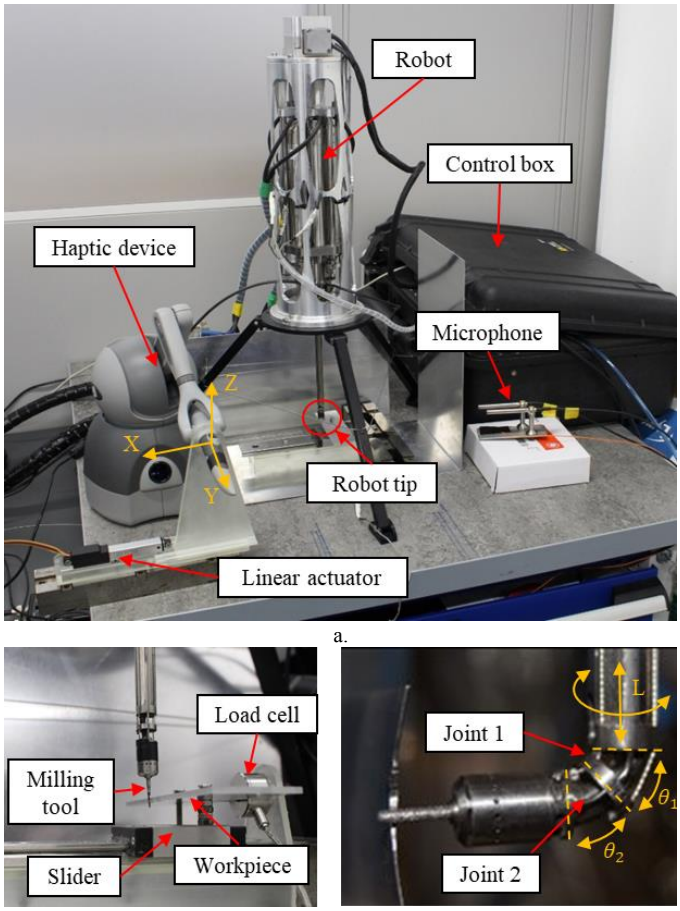

Fig. 4. System hardware: a. Main components of the system, with haptic device, robot actuation and sound acquisition system; b. A detailed view of the end-effector and the workpiece setup with a load cell to measure the radial milling force for a calibration experiment; c. End-effector of the robot in a bent position with the degrees of freedom of the system highlighted.

2) Haptic interface

The haptic interface provides direct interaction with the machine operator. A bilateral haptic coupling is used between the haptic device and the teleoperated robot. When the operator moves the haptic controller, the device continuously sends commands to the robot while receiving force feedback from the sound processing block. The haptic device used in the reported setup, by 3D SYSTEMS, has a refresh rate of 1000 Hz.

3) Robot teleoperation

The robot in this example has been designed for the in-situ repair of aerofoil [17][24]. As shown in Fig. 4c, the robot has four degrees of freedom: rotation around and translation along its base axis, and two bending degrees of freedom provided by nitinol compliant joints (joint 1 and joint 2 in Fig. 4c). In this work, only three degrees of freedom are used: bending angles θ_1 and θ_2 and linear motion L (see Fig. 4c). Thus, the three degrees of freedom of the haptic device (in Fig. 4a) can be mapped with a biunivocal relation onto the three motion variables of the robot. The Z-axis of haptic device is linked to the linear feed of the robot (L), while motion along the X- and Y-axes controls tip orientation, coupling the bending degrees of freedom (θ_1, θ_2). This coupling can be expressed with a simplified kinematic transformation, defined as

$$\begin{bmatrix}\theta_1\\ \theta_2\\ L\end{bmatrix} = \begin{bmatrix}t_x & 0 & 0\\ 0 & t_y & 0\\ 0 & 0 & t_z\end{bmatrix}\begin{bmatrix}X\\ Y\\ Z\end{bmatrix}, \quad (5)$$

where t_x, t_y, and t_z are scaling parameters between the workspace of haptic device and robot tip.

B. Machining sound acquisition and processing

This section introduces a method for machining force estimation from audible features with its application to our example. The robot in Fig. 4 is equipped with an air-driven machining tool for either milling or grinding. Such air-driven high-speed spindles are characterized by a near-linear torque-speed relation [23], and any force applied to the robot end-effector, including contact reaction forces, decreases spindle rotation velocity and sound frequency. Thus, the radial force applied to an air-driven spindle can be estimated from its rotation frequency during grinding or milling, which are the most common operations in aeroengine repair. The relationship between those variables can be experimentally obtained for a known workpiece and machining tool [18].

To obtain an accurate radial machining force from sound features, we propose a method which can be implemented into any existing machining system in two steps: an online acquisition of the sound signal generated during the machining process with real-time detection of the spindle frequency; and an offline mapping of radial milling/grinding force and spindle frequency, which requires prior calibration.

1) Online spindle frequency acquisition

The sound generated by a milling/grinding process is composed of four different main sources: the collision between the machining tool and workpiece; the rotation of the spindle turbine when driven by compressed air; background noise; and the exhaust air blown out of the air-driven spindle. Only the sound that comes from the first source is needed, as this frequency is associated with the spindle's one, whereas the other three sound sources can be seen as external disturbances.

In the proposed example, the sound signal is sampled at 50 kHz by DAQ in LabVIEW, and the capture time is 0.002s at every loop (100 datapoints per capture window). For each acquisition, the power spectrum density (PSD) is calculated to detect the spindle frequency among the noise. An example of signal PSD plot from a milling operation on a titanium workpiece is reported in Fig. 5a. As highlighted in the graph, sound under 1000 Hz is considered background noise.

The two visible peaks indicate two distinct modes of the milling sound: the frequency of the first mode represents the spindle's dominant frequency, and the value of second mode is always double of the first mode (first harmonic). As the amplitude of machining sound decreases with the spindle frequency, it can become undetectable under a certain threshold (identified as 2000 Hz in the reported example), which is affected by environment noise and microphone position (150mm distance between microphone and machining tool in the reported example). As such, the distance between microphone and sound source should be minimized when possible to improve detection rate.

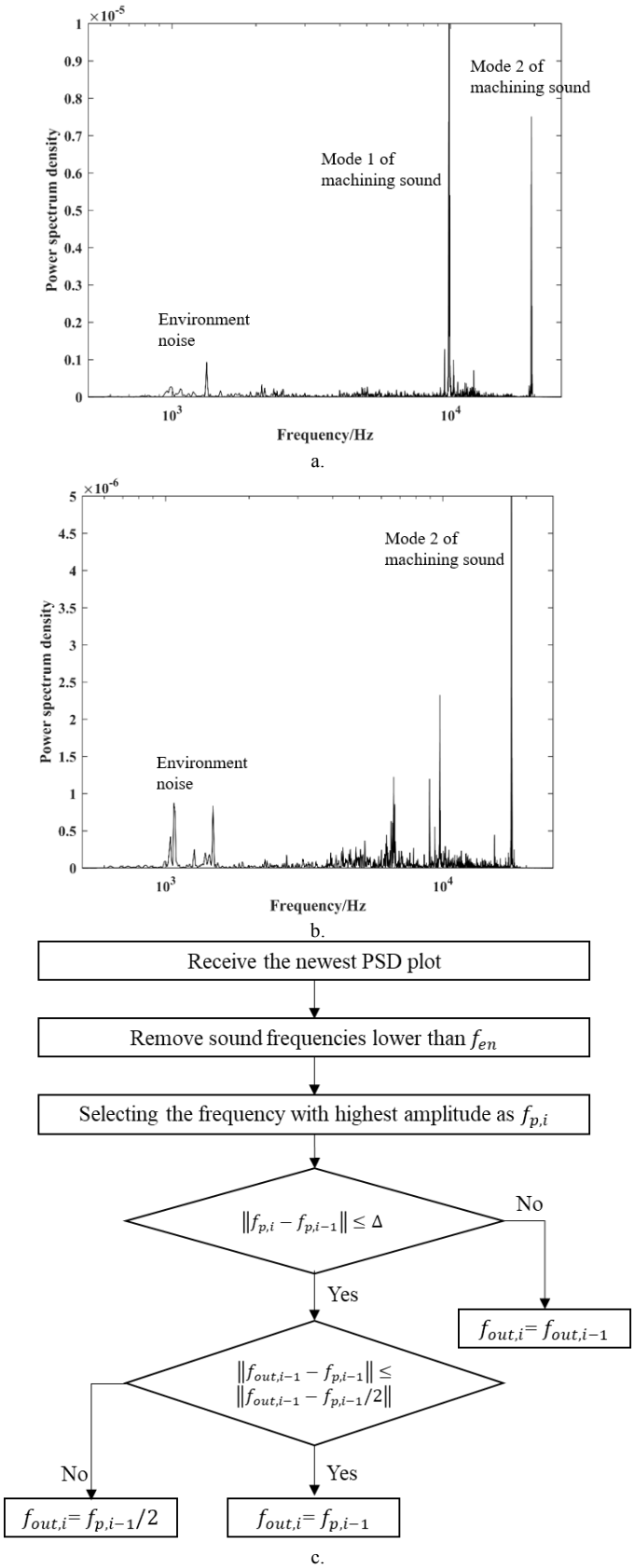

Fig. 5. Sound acquisition and processing: a. An example power spectral density plot at a frequency range from 0 to 20 kHz acquired for a Ti sample machined with a milling tool; b. An example PSD plot with different signal characteristics; c. The proposed spindle frequency tracking algorithm.

To enable the real-time detection of spindle frequency variation, the power spectral density is refreshed at 475 Hz. This refresh rate is determined by the need of acquiring enough samples to calculate the PSD-frequency plot and cannot be increased further without deteriorating signal quality. The spindle frequency is identified in every frame of power spectral density. This task is fairly easy when the PSD-frequency plot is always as clear as the example shown in Fig. 5a. However, undesired spindle vibrations (e.g. repeated collisions between machining tool and workpiece due to compliance in the fixtures), the natural frequencies of workpiece, and the noise produced by the exhaust air might muffle or fully cover one or more peaks during an individual update of the PSD plot due to its high refresh rate. For example, Fig. 5b is a such a plot with different signal characteristics, with several peaks around the first modal frequency that make it difficult to identify correctly. This causes conventional filters to be unreliable in their tracking. Therefore, an algorithm to track the dominant frequency variation correctly and stably is required.

We here propose a tracking algorithm that follows the flowchart in Fig. 5c. In every loop in which the PSD-frequency is calculated, the first step is removing environment noise, usually in the lower frequency range. In our environment, this background noise has been estimated to reach up to 1000Hz ($f_{en} = 1000\ Hz$). For the i^{th} loop of the algorithm, we compute the frequency of the peak with highest amplitude as $f_{p,i}$. To judge if $f_{p,i}$ represents a spindle's mode or noise, its value is compared with the peak frequency of the previous loop $f_{p,i-1}$. As the spindle frequency value should be continuous, the newly acquired $f_{p,i}$ is kept as a valid frequency only when its difference from $f_{p,i-1}$ is smaller than a given interval Δ (here set to 250 Hz after an experimental calibration). When this difference is higher than the threshold, we discard the acquired $f_{p,i}$ and keep using the value of $f_{p,i-1}$. If $f_{p,i}$ is identified as one of the modes of spindle frequency, we check which mode it is and consequently obtain the dominant frequency.

2) Calibration of machining force and spindle frequency

To estimate the machining force from the spindle frequency, the relationship between them should be mapped through an experimental calibration. Here we describe a calibration procedure to map radial machining force and spindle frequency when milling or grinding Ti and Al workpieces with the robot.

As described before, the haptic joystick's position in its own reference frame is mapped onto the robot tip's position in Cartesian space. Thus, the pose of the end-effector tool can be controlled by joystick movement. To execute accurate repeated trials, the haptic joystick is driven by a linear motor (Actuonix L12-50-100-12-P DC) at a constant velocity of 1 mm/s along a slider, as in Fig. 4. In each trial, the motor drives the joystick from its initial position, where the tool is not in contact with the workpiece, to the end position, where the tool has stalled.

The real-time radial force between the milling tool and the workpiece is measured by a load cell (LCMFD-10N). The workpiece (100 mm × 30 mm × 1.35 mm) is made of titanium and fixed on a slider (MISUMI SSE2BWLZ14G-160). When the milling tool engages the edge of the workpiece, its opposite

edge pushes onto the load cell to guarantee that the force measured by the load cell equals the radial milling force. The real-time milling frequency is also acquired and recorded by system. The trial has been repeated 25 times and every trial is conducted on a new (non-machined) contact point.

To obtain the relationship between frequency and radial force, the recorded frequency and radial force are synchronized and combined, and the correspondence between frequency and force value is identified for each frequency sample. In the example trials on the titanium workpiece, the sample frequency ranges from 3500 Hz to 16000 Hz with increments of 2500 Hz. After getting the data from all 25 trials, a fitting curve generated from their average value was identified. Fig. 6 shows the deviation in measured radial milling force for each sample frequency among all the trials, the average radial milling force value, and the fitting curve (in red), generated by using a polynomial function from the average radial force of all trials.

When the milling tool enters in contact with the titanium workpiece, the spindle frequency is about 17500 Hz, whereas the detectable lower limit frequency is 2000 Hz. In the range between 2000 Hz and 175000 Hz, the radial milling force has a near linear relationship with the spindle frequency.

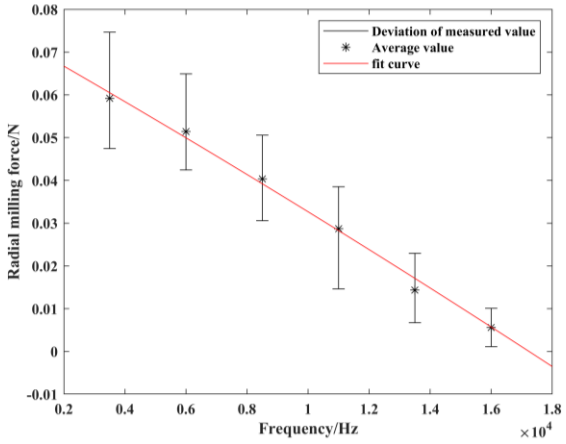

Fig. 6. Measured frequency and corresponding force. Each black bar indicates the result deviation of all trials, each black point indicates the average value at a given frequency, and the red curve fits the average values.

C. Haptic force feedback

The haptic force feedback is designed according to the principle described in Section II, with two modes employed to ensure that the user feels the machining force while keeping the system both safe and stable. When the robot tip is not in contact with the workpiece, the system works in motion control mode as described in Section II and a spring-like force is generated as

$$F_H^I = k_I \cdot (P_H^E - P_H^I) \quad (6)$$

where F_H^I is the haptic feedback force, $P_H^E \in \mathbb{R}^3$ is the position vector in the haptic device coordinate system calculated from the current actuator position, $P_H^I \in \mathbb{R}^3$ is the commanded position in the haptic device coordinate system, and $k_I \in \mathbb{R}$ is a linear scaling factor used to amplify the low operation forces up to a value that an operator can easily feel. In this example, $k_I = 5\ \mathrm{N/mm}$ is selected as comfortable for the user to operate.

When the robot starts machining, the process sound frequency is detected, and the force feedback is obtained as

$$F_H^I = k_{II} \cdot R_{EtoH} \cdot F_M \quad (7)$$

In this stage, F_M is the radial machining force, $R_{EtoH} \in SO(3)$ is the rotation matrix from the robot's frame to the haptic device's frame, and k_{II} is an adjustable scaling factor to amplify the force for an improved user experience. For the experiments in this paper, considering the range of F_M and haptic device specifications ("3D System", maximum feedback force of 3.3 N), k_{II} is set to a standard of 30 to amplify the feedback force to a suitable range in which operator can feel the feedback force variety clearly. For an improved sensitivity in a lower force range, higher values (e.g. 100) can be selected, but they lead to force feedback saturation in the higher force range.

Apart from the above stages, a third feedback mode is introduced to prevent stalling. If the measured sound frequency is lower than a critical limit frequency, close to the stall position as measured in the calibration experiment or out of the system detection range, our system creates a "virtual wall" to stop user from going closer to stall or uncontrolled operation. The further an operator moves the haptic joystick in the critical direction, the stronger the haptic force added to stop motion. When moving in any other direction (thus farther from risk), no force is experienced. This haptic force F_H^I is defined as

$$F_H^I = \begin{cases} k_{III}(P_H^I - P_H^S), & r \cdot R > 0 \\ 0, & r \cdot R \le 0 \end{cases} \quad (8)$$

where P_H^S is the haptic device position recorded when the signal reached the alert area, $r \in \mathbb{R}^3$ is the direction of motion of the haptic device, $R \in \mathbb{R}^3$ is the force vector mapped in the haptic reference frame, and $k_{III} = 20\ \mathrm{N/mm}$ is the stiffness of the haptic "virtual wall". This force feedback at different stages is summarized in Fig. 7, where $f_{initial}$ represent the lower boundary of the sound frequency when no external force acts on the machining tool and $f_{alert} = 2000\ \mathrm{Hz}$ is the lower frequency that the system can reliably detect without risking stalling or the environmental noise covering the first mode of the tool's frequency. The user is thus alerted with the strong feedback of the stiff virtual wall.

Even though the example system uses the control architecture shown in Fig. 2, due to hardware limitations the three control blocks described above have different update rates: the update rate of block A is about 500 Hz, limited mainly by the sample time of the sound signal acquisition; block B runs at 1000 Hz, a commonly used refresh rate for haptic devices; and block C is updated at 400 Hz, mainly constrained by the computational time needed to solve robot kinematics. Thus, the system runs the three loops in an asynchronous execution.

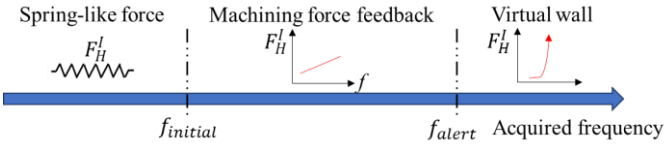

Fig. 7. Feedback force strategy for the machining application example.

IV. Experimental Validation

In this section, two sets of experiments are carried out to evaluate the performance of the proposed method in the example from Section III: a calibration test to map force to acquired sound, and a demonstration of the system.

A. *Machining force estimation test*

To obtain the relationship between force and spindle frequency, we have repeated the experimental calibration process in Section III for three scenarios: milling and grinding titanium and milling aluminum. Each trial was repeated 25 times, with results in Fig. 8 and Table II. The curves in Fig. 8a are generated by a simple interpolation, but machine learning could be used for a more accurate estimation. The three curves fit the average radial force value, showing a similar near linear behavior for each configuration, validating our force estimation method for different processes and materials. In Fig. 8b-d, the error between estimated (sound-based) and acquired (load cell) radial milling force is shown. In the figures, red lines represent the mean error (100% trials), black boxes describe the force error deviation (80% trials, no outliers), and the dotted line shows the error limit (100% trials). This error is caused by background noise and load cell vibration due to impacts and compliance of the machining tool. The aluminium milling experiment shows the largest relative error due to its weaker sound intensity and smaller machining force range. A similar behavior is expected for other materials, with softer material showing a higher error.

B. *System demonstration*

To verify the performance of the proposed system in a real-case scenario, the robot was controlled manually to mill the edge of a titanium workpiece, with the experimental setup shown in Fig. 10. In this demonstration, an operator moves the haptic joystick along its X-axis, teleoperating the robot in a milling operation on the workpiece's edge along the X-axis of the robot's frame. The radial milling force is acquired with a load cell, and the motion of the tool is measured by a VICON motion capture system with 4 Vantage cameras as ground truth. Meanwhile, the joystick position and the force feedback are recorded and reported in Fig. 10 for a milling task over a length of 9 mm in 90 s (Fig. 9c). Comparing this to the ground truth highlights the linear mapping between the commanded pose in the haptic frame and the corresponding tip pose in the robot frame. Thus, the robot followed the haptic command accurately, with a limited motion difference when the operator "forces" the robot to move against a physical boundary. The comparison between the milling force estimated through audible sound features (from which the haptic feedback force is obtained) and the load cell acquisition in Fig. 10 shows a negligible error between the estimated and measured force, smaller than 0.01 N.

TABLE II
FREQUENCY AND FORCE LIMITS FOR THE REPORTED CONFIGURATIONS

Configuration	Frequency limit (Hz)	Force limit (N)	Mean error
Milling, Titanium	17500	0.075	6%
Grinding, Titanium	15000	0.105	11%
Milling, Aluminum	12500	0.045	20%

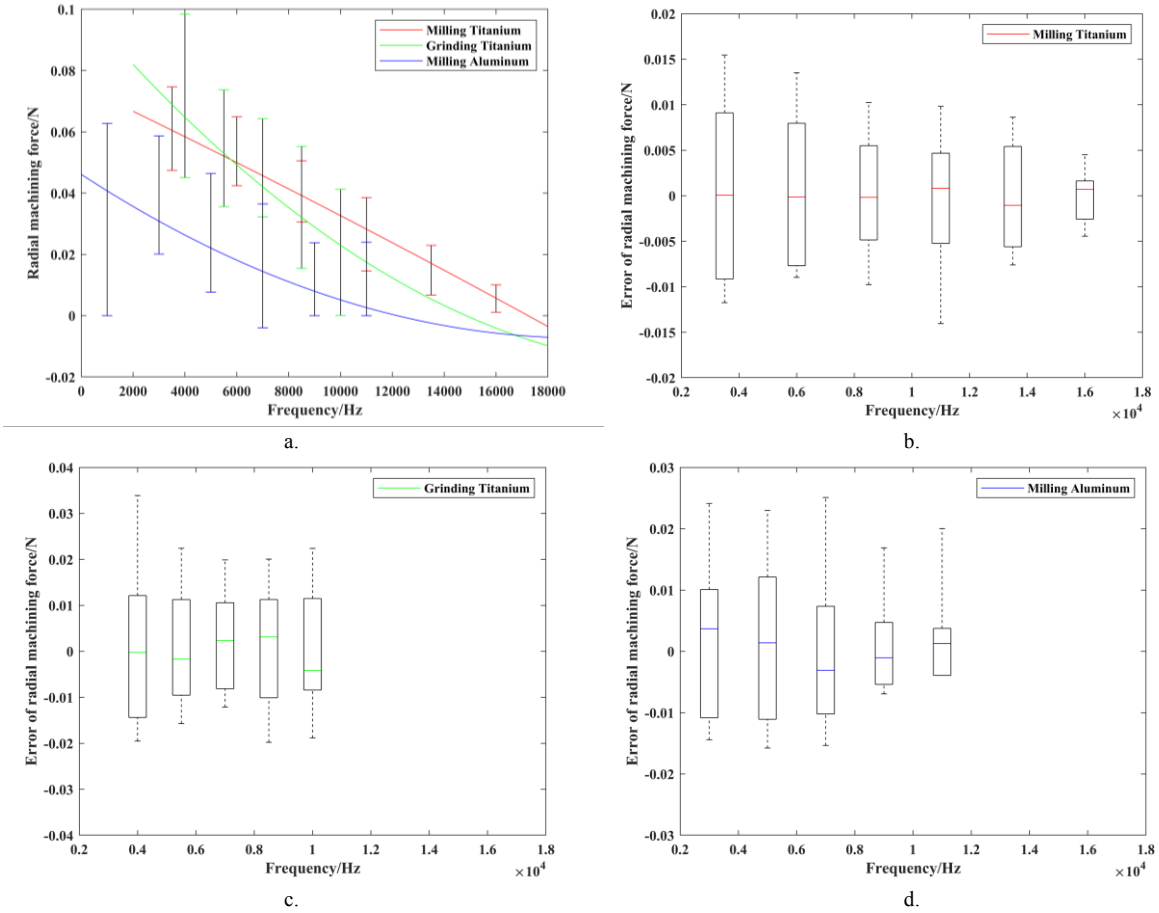

Fig. 8. Estimation of radial machining force: a. Radial machining force acquired at different frequencies for three processes (average fit as curves, acquired result deviation as bars); b. Analysis of the error between estimated force and measured force in titanium milling trials; c. Error result of titanium grinding trials; d. Error result of aluminum milling trials.

C. Discussion

As shown in the specific example in this section, the proposed haptic teleoperation method makes an operator able to "touch" the sound generated by a machining task. For in-situ repairs, installing any internal/on-board sensor is often difficult or impossible, but this method enables an easy acquisition with an external microphone without changes to the system or the environment. The machining tool's spindle frequency can be then extracted to derive the wrench acting on the system and feed it back to the user in real time. Therefore, the system achieves haptic control through a sound signal only. In the proposed example, enabling haptic control helps operators to control machining force and avoid tool stall. This result proves the feasibility of using audible features to estimate an otherwise unknown force and increase operation performance.

1) Experimental errors

The spindle frequency against radial force plot in the three reported conditions have similar trends, with an error distribution ranging between 0.01 N and 0.02 N. Two main causes for error can be found in equipment performance and time delay. The first error source is due to the vibration caused by the contact between the machining tool and workpiece, which causes a noise peak on the load cell signal (see Fig. 10), which hinders the identification of an exact measurement result.

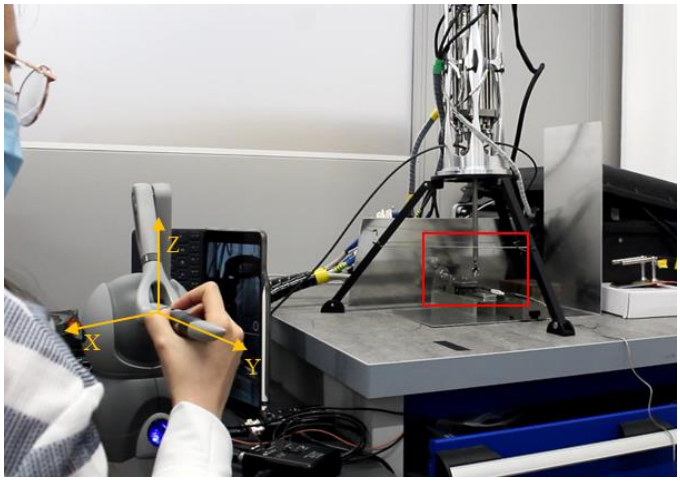

a.

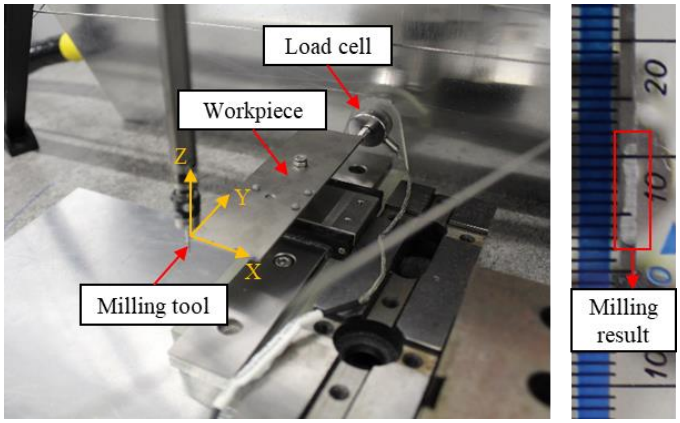

b.

c.

Fig. 9: System demonstration: a. An operator milling the edge of the workpiece by using the haptic device; b. A detailed view of the end-effector and the workpiece setup with a load cell to measure the radial milling force; c. Resulting material removal on the workpiece.

The second error cause is the time delay between force measurement and spindle frequency detection. The acquisition and processing of the sound signal consumes time every loop, and the estimated force is always slightly delayed when compared to the load cell real-time measurement.

2) Performance during manual operation

The system is designed to teleoperate the robot manually and make the user feel the force extracted from the acquired sound. With the proposed demonstration in a realistic scenario, the system proved capable of realizing stable and accurate motion control, preventing the user from stalling or moving the robot to a critical configuration. As shown in Fig. 10, the robot tip position followed the command position from the haptic device with a negligible time delay. From the aspect of haptic force feedback, the system can acquire the radial machining force with a small error during manual operation, and the corresponding feedback can be tuned by the operator to a comfortable value, which might vary from person to person.

3) System limitations

Regarding sound signal acquisition stability, the proposed example is limited in two situations: first, when the machining tool spindle rotation frequency is too low, its amplitude in power spectrum density plot is exceeded by the external noise, preventing force estimation with the proposed method; moreover, the sound signal is affected by external factors such as the vibration of the robot tip and the distance between the sound source and the microphone. In future developments, an improved signal processing algorithm that considers these factors could increase the robustness of the system.

Another limitation of the reported example is the focus on the relationship between radial machining force and spindle frequency without considering other force components (or moments) acting on the system. For the example in this work, while negligible, these other components are still present and could have increased the uncertainty during both calibration and operation. In future works, to improve the system force feedback, other components of the wrench (e.g., tangential force) will be considered and implemented to provide the user with a better "feeling" of the operation. This limitation also constrains the robot to machine the workpieces along simple paths, whereas a better control over complex shapes can be enabled with multi-axial feedback.

4) Applications

This example tests the force estimation accuracy on repetitive trials that measure radial force from free spindle rotation at maximum velocity to system stall. As shown by the implementation of the *touching the sound* algorithm in three different conditions (i.e. milling a titanium workpiece, grinding a titanium workpiece, and milling an aluminum workpiece), the proposed method can be adapted to a variety of machining operations and materials. While not demonstrated in this work, we expect that these results can be expanded to any task with an established relation between sound features and force. By enabling haptic feedback, this method has the potential to improve operation control in highly constrained environments, with potential for both medical and industrial applications.

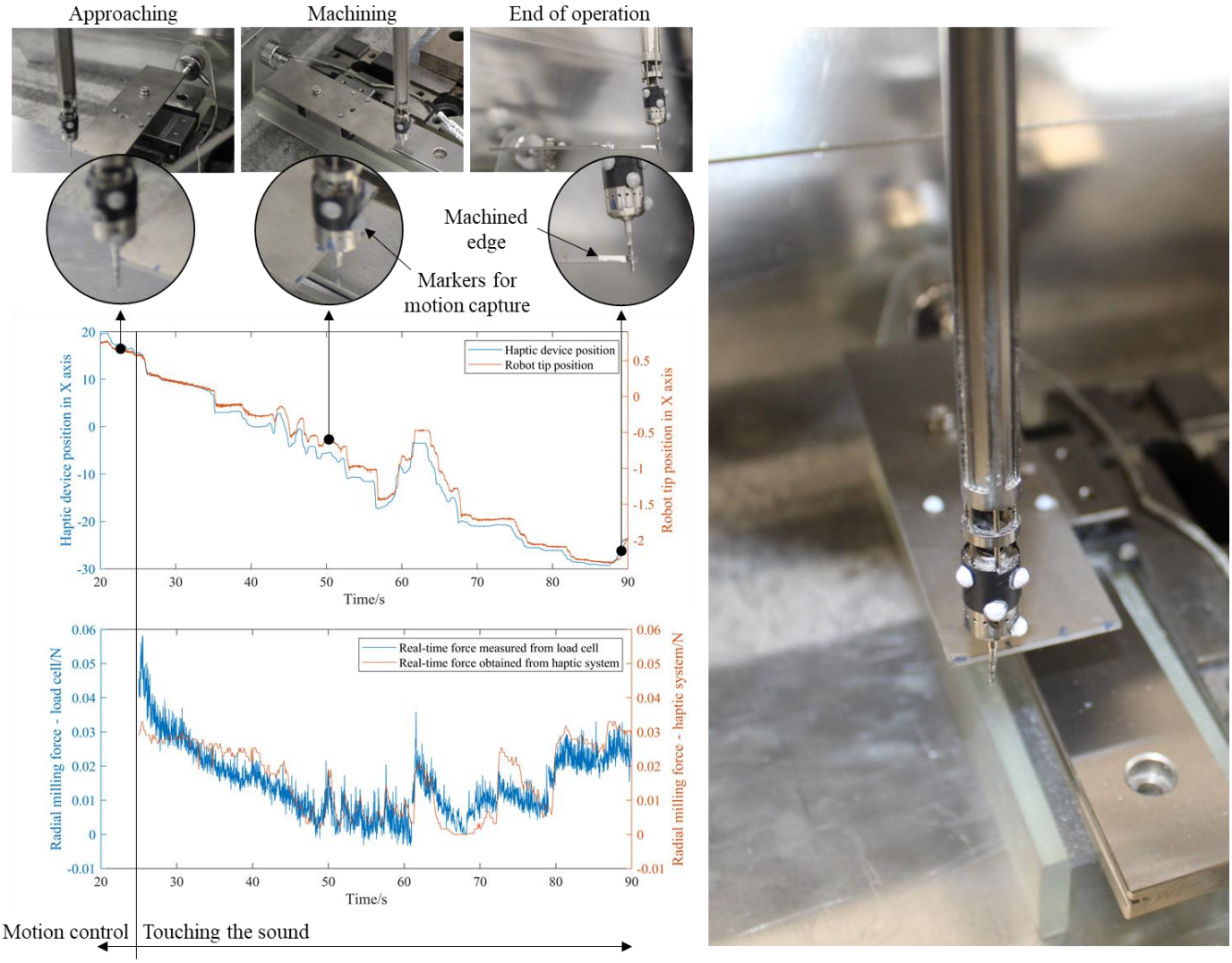

Fig. 10. Results from system demonstration.

V. Conclusion

Haptic interfaces can significantly assist a human operator in assessing the force transmission between a robot and the environment during remote operation, when the operator cannot see or hear the process, thus improving performance. The main challenge is how to obtain the force applied to the robot end-effector when both the robot and its workspace cannot include conventional sensors. To solve this issue, we propose a novel haptic control method based on acoustic emissions.

The proposed system acquires force by using audible sound features in an environment with no other sensor than a microphone, which can also be deployed remotely as long as the sound is audible. An example prototype was developed and validated for machining applications. The contributions of this work are outlined in the following points:

- A novel haptic control system that can teleoperate a robot and provide users with a real-time force feedback from process-generated sound has been introduced.
- The force estimation accuracy of the proposed method is experimentally measured for example scenarios. In particular, machining applications have been reported with three different configurations of tool and workpiece material: milling a titanium workpiece, grinding a titanium workpiece, and milling an aluminum workpiece. The maximum measured force error in the three cases is 0.015 N (20%), 0.02 N (19%), and 0.025 N (44%) respectively, which compare favorably to similar systems for indirect force estimation.
- Haptic control performance is verified in terms of motion following and force estimation capability during an example operation. The system is proved to correctly follow the input motion and estimate the force with negligible errors and delay.

Overall, the method developed in this paper presents promising results for the addition of haptic feedback when no conventional force sensors can be introduced in the system. The proposed method has been demonstrated as reliable over a range of real-case scenarios, with a timely motion control and real-time force acquisition and feedback to the operator.

References

[1]. E. Steinbach et al., "Haptic Communications," *Proceedings of the IEEE*, vol. 100, no. 4, pp. 937-956, Apr. 2012.

[2]. G. Garcia-Valle, M. Ferre, J. Brenosa, and D. Vargas, “Evaluation of ˜ presence in virtual environments: Haptic vest and user’s haptic skills,” *IEEE Access,* vol. 6, pp. 7224–7233, Dec. 2018.
[3]. Luis Pérez, Eduardo Diez, Rubén Usamentiaga, Daniel F. García, “Industrial robot control and operator training using virtual reality interfaces,” *Computers in Industry,* vol. 109, pp. 114 – 120, Aug. 2019.
[4]. A. Hooshiar, S. Najarian and J. Dargahi, "Haptic Telerobotic Cardiovascular Intervention: A Review of Approaches, Methods, and Future Perspectives," *IEEE Reviews in Biomedical Engineering,* vol. 13, pp. 32-50, Apr. 2020.
[5]. N. Enayati, E. De Momi and G. Ferrigno, "Haptics in Robot-Assisted Surgery: Challenges and Benefits," *IEEE Reviews in Biomedical Engineering*, vol. 9, pp. 49-65, 2016.
[6]. R. Xu, A. Yurkewich and R. V. Patel, "Curvature, Torsion, and Force Sensing in Continuum Robots Using Helically Wrapped FBG Sensors," in *IEEE Robotics and Automation Letters*, vol. 1, no. 2, pp. 1052-1059, July 2016.
[7]. W. Lai *et al*., "Force Sensing With 1 mm Fiber Bragg Gratings for Flexible Endoscopic Surgical Robots," in *IEEE/ASME Transactions on Mechatronics*, vol. 25, no. 1, pp. 371-382, Feb. 2020.
[8]. H. Wang, Z. Yan, Y. Gao, W. Wang and Z. Du, "3-D Force Sensing Strategy of Laryngeal Continuum Surgical Robot Based on Fiber Bragg Gratings," in *IEEE Transactions on Instrumentation and Measurement*, vol. 70, pp. 1-10, 2021.
[9]. Khan, R. J. Roesthuis and S. Misra, "Force sensing in continuum manipulators using fiber Bragg grating sensors," *2017 IEEE/RSJ International Conference on Intelligent Robots and Systems (IROS)*, 2017, pp. 2531-2536
[10]. L. Van Duong and V. A. Ho, "Large-Scale Vision-Based Tactile Sensing for Robot Links: Design, Modeling, and Evaluation," in *IEEE Transactions on Robotics*, vol. 37, no. 2, pp. 390-403, April 2021.
[11]. G. Fagogenis, M. Mencattelli, Z. Machaidze, B. Rosa, K. Price, et al.. Autonomous robotic intracardiac catheter navigation using haptic vision. Science Robotics, American Association for the Advancement of Science 2019, 4 (29), pp.eaaw1977.
[12]. K. Xu and N. Simaan, “An investigation of the intrinsic force sensing capabilities of continuum robots,” *IEEE Transactions on Robotics,* vol. 24, no. 3, pp. 576–587, 2008.
[13]. R. Roy, L. Wang, and N. Simaan, “Investigation of effects of dynamics on intrinsic wrench sensing in continuum robots,” in *2016 IEEE International Conference on Robotics and Automation (ICRA),* Stockholm, Sweden, 2016, pp. 2052–2059.
[14]. D. Jakes, Z. Ge and L. Wu, "Model-less Active Compliance for Continuum Robots using Recurrent Neural Networks," in *2019 IEEE/RSJ International Conference on Intelligent Robots and Systems (IROS),* Macau, China, pp. 2167-2173, 2019.
[15]. A. Mohammad, M. Russo, Y. Fang, X. Dong, D. Axinte, J. Kell, “An efficient follow-the-leader strategy for continuum robot navigation and coiling.” *IEEE Robotics and Automation Letters* 6, no. 4 (2021): 7493-7500.
[16]. M. Russo, N. Sriratanasak, W. Ba, X. Dong, A. Mohammad, D. Axinte, “Cooperative continuum robots: Enhancing individual continuum arms by reconfiguring into a parallel manipulator”, *IEEE Robot. Autom. Lett.* vol. 7, no. 2, pp. 1558-1565, 2022, doi: 10.1109/LRA.2021.3139371.
[17]. D. Alatorre, B. Nasser, A. Rabani, A. Nagy-Sochacki, X. Dong, D. Axinte, and J. Kell, “Teleoperated, in situ repair of an aeroengine: Overcoming the internet latency hurdle,” *IEEE Robotics & Automation Magazine,* vol. *26*(1), pp.10-20, 2018.
[18]. D. Alatorre, A. Rabani, D. Axinte, and D. T. Branson, “Closed loop force control of in-situ machining robots using audible sound features,” *Mechanical Systems and Signal Processing,* vol. 136, pp. 106517, 2020.
[19]. Rubio, E.M., Teti, R. “Cutting parameters analysis for the development of a milling process monitoring system based on audible energy sound,” *Journal of Intelligent Manufacturing,* vol. 20, no. 43, pp. 43-54, 2009.
[20]. V. Nasir, J. Cool, and F. Sassani, “Intelligent machining monitoring using sound signal processed with the wavelet method and a self-organizing neural network,” *IEEE Robotics and Automation Letters,* vol. 4, no. 4, pp. 3449–3456, 2019.
[21]. T. L. Schmitz, M. A. Davies, and M. D. Kennedy, “Tool Point Frequency Response Prediction for High-Speed Machining by RCSA ,” *Journal of Manufacturing Science and Engineering,* vol. 123, pp. 700–707, 2001.
[22]. C. Liu, G.F. Wang, X.D. Qin, L. Zhang, “The online monitoring of surface quality based on time-frequency spectrum analysis of acoustic emission,” *Applied Mechanics and Materials.* Vol. 141, pp. 564–568, 2012.
[23]. J.E. Dyson, B.W. Darvell, “Torque, power and efficiency characterization of dental air turbine handpieces,” *Journal of Dentistry,* vol 27, issue 8, pp. 573-586, 1999.
[24]. M. Russo, L. Raimondi, X. Dong, D. Axinte, and J. Kell, “Task-oriented optimal dimensional synthesis of robotic manipulators with limited mobility,” *Robotics and Computer-Integrated Manufacturing,* vol 69, p.102096, 2021.